

# Finite-size scaling analysis of percolation in three-dimensional correlated binary Markov chain random fields

Thomas Harter

University of California, Davis, California 95616-8628, USA

(Received 26 December 2004; published 18 August 2005)

Percolation and finite-size scaling properties in three-dimensional binary correlated Markov-chain random fields on a cubic lattice are computed by extensive Monte Carlo simulation. At short correlation scales, the percolation threshold in correlated random fields decreases as the correlation scale increases. The rate of decrease rapidly diminishes for correlation lengths larger than 2–3 lattice sites. At correlation scales of 4–6 lattice sites, the percolation threshold is found to be  $0.126 \pm 0.001$  for the Markov chain random fields, similar to that for sequential Gaussian and indicator random fields, which are evaluated for comparison. The average percolation threshold in finite-size lattices is a function of both, the correlation length and the finite lattice size. The universal scaling constants for mean cluster size and backbone fraction are found to be consistent with results on uncorrelated lattices. But prefactors of scaling relationships vary with correlation length. The squared radius of gyration of nonpercolating clusters is found to scale with  $\gamma/\nu$  and its scaling prefactors are independent of the correlation scale. Prefactors are similar between the three random field generators evaluated. The percolation properties derived here are useful to account for finite-size effects on percolation in natural or manmade correlated systems.

DOI: [10.1103/PhysRevE.72.026120](https://doi.org/10.1103/PhysRevE.72.026120)

PACS number(s): 05.70.Jk, 05.50.+q, 47.55.Mh, 64.60.Ak

## INTRODUCTION

Percolation phenomena in random (disordered) media have been extensively studied in a wide variety of fields including physics, chemistry, engineering, and life, earth, and environmental sciences [1]. Emphasis has been given to percolation properties of uncorrelated random media. For uncorrelated systems, percolation thresholds and critical behaviors near the percolation thresholds are well known [2]. Less attention has been given to percolation properties of media with short- or long-range correlations [3–5], particularly in three-dimensional systems [6,7]. Yet, three-dimensional spatial correlations within the disorder of random media are intrinsic to most natural systems and also to many artificial (manmade) systems.

The critical behavior in media with short-range correlations is thought to be identical to that in uncorrelated systems [4,8]. However, the percolation threshold  $p_c$ , which is 0.3116 in uncorrelated three-dimensional cubic lattice media [2], has been observed to vary with the correlation scale  $\lambda$  and also with the system type (lattice type, random field type). There is no universal three-dimensional percolation threshold for correlated, infinite random media systems, although it is generally known that correlations reduce the percolation threshold [1,9–11] and affect prefactors in scaling laws. For long-range correlations and in small finite-size systems, the scaling exponents themselves can be different from those of uncorrelated lattices [4,5].

Disordered media with a finite length scale (spatial extent)  $L$  and with short-range correlations characterized by a finite correlation scale  $\lambda$  are intrinsically finite with respect to the amount of structure observed within the medium (unless it is hierarchical or fractal). Unlike in media with uncorrelated structures, finite-size effects may therefore play a significant role in many natural or engineered disordered, correlated systems [12,13].

In finite-sized random binary systems, the occurrence of percolation is associated with a probability  $\Pi$ , which continuously varies with the fraction  $p_1$  of “occupied” or “conductive” sites. The value of  $p_1$  for which the probability of percolation is 50% is sometimes referred to as the finite-sized percolation threshold or, more commonly, the average percolation threshold  $p_{av}$ . In general,  $p_{av} > p_c$  and  $p_{av} \rightarrow p_c$  for  $L \rightarrow \infty$ . The average percolation threshold  $p_{av}$  depends not only on the lattice size  $L$ . It has recently been pointed out that  $p_{av}$  of three-dimensional finite-sized systems decreases with increasing correlation scale  $\lambda$  [14–16], although these efforts were inconclusive and based on either a very small number of Monte Carlo realizations or based on relatively small lattice sizes or both.

The purpose of this paper is to further characterize the percolation behavior of finite-sized binary random fields on cubic lattices using Monte Carlo simulations with a sufficiently large number of realizations and relatively large lattices (up to  $201^3$ ). The paper explores the specific percolation properties of Markov-chain random fields (see below). Markov-chain random fields are typically used, e.g., to represent heterogeneous geologic media [17,18]. Here, I am specifically interested (1) to determine whether  $p_{av}(\lambda)$  of the Markov-chain fields is similar to that of Gaussian random fields; (2) to identify the approximate shape of  $\Pi$  as a function of  $\lambda$ ; and (3) to analyze the finite-sized behavior of the backbone fraction of the percolating cluster  $P_\infty$ , the mean cluster size  $S$ , and the connectivity length or cluster radius of gyration  $\xi$ , near  $p_{av}$  as a function of  $\lambda$ . In infinite systems, these are known to scale according to

$$P_\infty \sim |p - p_c|^{-\beta}, \quad (1)$$

$$S \sim |p - p_c|^{-\gamma}, \quad (2)$$

$$\xi \sim |p - p_c|^{-\nu}, \quad (3)$$

where the so-called critical exponents  $\beta$ ,  $\gamma$ , and  $\nu$  are universal constants. For uncorrelated infinite three-dimensional systems, the exponents are known to be 0.41, 1.8, and 0.88, respectively. It has been postulated that these exponents are independent of the lattice type or the correlation scale, if the latter is short ranged [4]. In finite-sized systems, knowledge of the prefactors (proportionality constants) in the above relationships is of importance and I present these as functions of the correlation scale.

### MONTE CARLO SIMULATIONS

Correlated binary random fields  $Z$  on a simple cubic lattice are generated using a first-order Markov-chain model. First-order Markov-chain random fields are defined by the proportion  $p_j$  of each phase  $\omega_j$  and the stationary transition probability  $t_{j,k}(\mathbf{h}_\Phi)$  in each of three directions  $\Phi$  spanning a three-dimensional space  $\Phi \in \{1, 2, 3\}$ . The transition probability is defined as

$$t_{j,k}(\mathbf{h}_\Phi) = P(Z(\mathbf{x} + \mathbf{h}_\Phi) = \omega_k | Z(\mathbf{x}) = \omega_j) \quad \text{for all } \mathbf{x}, (\mathbf{x} + \mathbf{h}_\Phi) \in \Omega. \quad (4)$$

$P(\cdot | \cdot)$  is a conditional probability,  $\mathbf{h}_\Phi$  is a separation vector in the direction  $\Phi$ ,  $Z(\mathbf{x})$  is the random phase at location  $\mathbf{x}$ , and  $\Omega$  is the finite-size three-dimensional simulation domain [19]. Transition probabilities are a function of the mean length  $\Lambda_{\Phi,j}$  of phase  $\omega_j$  such that

$$\Lambda_{\Phi,j} = -[\partial t_{j,j}(0)/\partial \mathbf{h}_\Phi]^{-1}. \quad (5)$$

Three-dimensional random fields are generated by first computing the Markov-chain transition rate matrices in the three principal lattice dimensions from the transition probability matrices, and then applying ellipsoidal interpolation to compute transition probabilities in any arbitrary direction during the sequential simulation step. The random field realization is optimized by simulated quenching to achieve a close fit of the sample statistics to the desired transition probability statistics [20].

In binary media [ $Z(\mathbf{x}) \in \{0, 1\}$ ], the first order Markov-chain random field exhibits an exponential covariance [21]:

$$\langle Z(\mathbf{x})Z(\mathbf{x} + \mathbf{h}) \rangle = p_1(1 - p_1)\exp(-|\mathbf{h}|/\lambda) \quad (6)$$

where  $\lambda = [(1 - p_1)\Lambda_{\Phi,1}]$  is the correlation length of  $Z$ . When the latter equation is used in conjunction with kriging analysis to generate realizations of a binary random field (rather than using the transition probabilities), the method is referred to as indicator simulation [22].

The transition probability Markov-chain (TPMC) random field generator [20] was used for Monte Carlo simulation of three-dimensional isotropic binary random fields on a simple cubic lattice with identical lattice size  $L$  in all three dimensions. Simulations were performed for  $L \in \{11, 21, 51, 101, 201\}$ . For each lattice size, uncorrelated random fields (using a uniform random number generator) and correlated random fields (using the TPMC method) with isotropic omnidirectional mean lengths  $\Lambda_1 \in \{1, 2, 4, 6\}$  are

generated at various  $p_1$ . The nondimensional  $\Lambda_1$  is the mean length normalized by the distance between neighboring sites on a cubic lattice. For comparison, a subset of these simulations was repeated using the sequential Gaussian and sequential indicator simulation algorithms [22].

All simulations were initially performed with a low number of realizations for each of  $p_1^{input} \in \{0.100, 0.101, 0.102, \dots, 0.399, 0.400\}$  to determine the approximate location of  $p_{av}$ , then a large number of realizations were performed for various  $p_1^{input}$  near the approximate  $p_{av}$  to obtain accurate estimates of  $p_{av}$  and the percolation properties at  $p_{av}$ . The number of increments in  $p_1^{input}$  at which Monte Carlo simulations were performed and the number of realizations per Monte Carlo simulation varied depending on the lattice size and mean length (Table I). Larger lattice size and mean lengths required a lower number of realizations to obtain similarly accurate results, but both also increased computational cost.

Percolation properties on each realization were analyzed using the Hoshen-Koppelman algorithm [2,23]. This included a check for the occurrence of percolation, the backbone fraction of the percolation cluster  $P_\infty$  (if it existed), the mean nonspanning cluster size  $S$ , and the mean connectivity length  $\xi$ . For individual realizations, these were computed from [23]

$$P_\infty = s_\infty/p_1, \quad (7)$$

$$S = \langle s^2 \rangle / \langle s \rangle, \quad (8)$$

$$\xi^2 = \langle \mathbf{x}^2 \rangle - (\langle \mathbf{x} \rangle)^2, \quad (9)$$

where  $s_\infty$  is the number of sites in the spanning cluster,  $s$  is the number of occupied sites in an individual nonspanning cluster,  $\mathbf{x}$  is the position vector of individual lattice points in the largest nonspanning cluster, and  $\langle \cdot \rangle$  indicates the expected value (arithmetic average) over all nonpercolating clusters (to compute  $S$ ) or over all cluster sites in the largest nonspanning cluster (to compute  $\xi^2$ ).

Measures of the first two central moments of  $d\Pi/dp_1, p_{av}$ , and  $\Delta$  were computed by first solving

$$p_{av}(L) \equiv \Pi^{-1}(0.5, L), \quad (10)$$

and then by determining the slope of  $\Pi$  at  $p_{av}$ :

$$1/\Delta(L) \equiv d\Pi(p_{av}(L), L)/dp_1. \quad (11)$$

The latter measure,  $\Delta(L)$ , is a representative measure of the range of  $p_1$  over which there is significant uncertainty about the existence of a spanning cluster in a given realization, in other words, the range over which the probability for percolation is significantly different from 0 or 1. The two moments can be applied to approximate  $\Pi(L)$  at any arbitrary  $L$  and  $\Lambda_1$  by using a Gaussian cumulative distribution function [24,25]  $G$ , with mean  $p_{av}(L)$  and variance  $\{2\pi\Delta^2(L)\}$ :

$$\Pi(L) \approx G(p_{av}(L), 2\pi\Delta^2(L)). \quad (12)$$

The percolation threshold,  $p_c$ , for an infinite system is obtained by fitting the data to the finite-size scaling equation [2]:

TABLE I. Setup of the numerical simulations. “RF method” refers to the random field generator used (U, uniform random number generator; TPMC, transition probability/Markov-chain generator; SI, sequential indicator generator; SG, sequential Gaussian generator with subsequent indicator cutoff conversion at that  $p_1$ th level of the cumulative probability distribution). For U, the column “Realizations” indicates the total number of realizations for which the percolation threshold was determined by varying the cutoff threshold  $p_1$ .

RF method	Domain length	Mean length	Increment of $p_1$	Realizations (per increment)	Lowest $p_1$	Highest $p_1$
U	5			100000	Iterative	
U	11			50000		
U	25			20000		
U	51			10000		
U	101			5000		
TPMC	11	1	0.002	25000	0.210	0.260
TPMC	21	1	0.002	10000	0.180	0.240
TPMC	51	1	0.001	5000	0.180	0.195
TPMC	101	1	0.001	5000	0.179	0.183
TPMC	11	2	0.002	25000	0.190	0.298
TPMC	21	2	0.002	10000	0.166	0.220
TPMC	51	2	0.001	3000	0.153	0.166
TPMC	101	2	0.001	2000	0.146	0.149
TPMC	11	4	0.001	20000	0.202	0.239
TPMC	21	4	0.001	10000	0.175	0.215
TPMC	51	4	0.001	1000	0.140	0.169
TPMC	101	4	0.001	2000	0.139	0.141
TPMC	201	4	0.001	100	0.131	0.145
TPMC	21	6	0.002	10000	0.180	0.236
TPMC	51	6	0.001	500	0.140	0.200
TPMC	101	6	0.001	500	0.140	0.154
TPMC	201	6	0.001	100	0.130	0.140
SI	51	4	0.001	1000	0.225	0.253
SI	101	4	0.001	300	0.186	0.206
SI	151	4	0.001	300	0.170	0.185
SG	51	10	0.001	1000	0.275	0.295
SG	101	10	0.001	300	0.200	0.238
SG	151	10	0.001	300	0.185	0.196

$$p_{av}(L) - p_c \sim \Delta(L). \quad (13)$$

The application of the universal scaling constants  $\nu$ ,  $\beta$ , and  $\gamma$  to Markov-chain random fields was tested by fitting the prefactors of the general scaling law for finite lattices to the simulation data using known values for the scaling constants (0.88, 0.41, 1.8, respectively):

$$p_{av}(L) - p_c \sim L^{-1/\nu} \quad \text{or} \quad \Delta(L) \sim L^{-1/\nu}, \quad (14)$$

$$\langle P_\infty(p_{av}(L), L) \rangle \sim L^{-\beta/\nu}, \quad (15)$$

$$\langle S(p_{av}(L), L) \rangle \sim L^{-\gamma/\nu}, \quad (16)$$

$$\langle \xi(p_{av}(L), L) \rangle \sim L^{-\nu/\nu}. \quad (17)$$

## RESULTS

### Percolation threshold $p_c$ of infinite uncorrelated and correlated systems

For the infinite lattice, finite-size scaling analysis of percolation in uncorrelated lattices yielded the percolation threshold to within 0.0005 of the known value and the exponent to within 5% of the known value: The fixed- $\nu$  method [Eq. (14)] yielded  $p_c=0.312$  while the variance method [Eq. (13)] yielded  $p_c=0.3116$  with  $\nu$  estimated at 0.92. In correlated lattices, the computed percolation threshold at  $\Lambda_1=1$  is significantly lower than in the uncorrelated lattice and decreases with increasing  $\Lambda_1$ . The rate of decrease rapidly diminishes for  $\Lambda_1>2$ . At  $\Lambda_1=6$ ,  $p_c$  is 12.6% ( $\pm 0.1\%$ ). This value is slightly higher than the 10.6%, 9.2%, and 9.4% estimated by Mendelson [16] for correlated random fields with Gaussian, exponential, and Laplace-Gaussian covariance

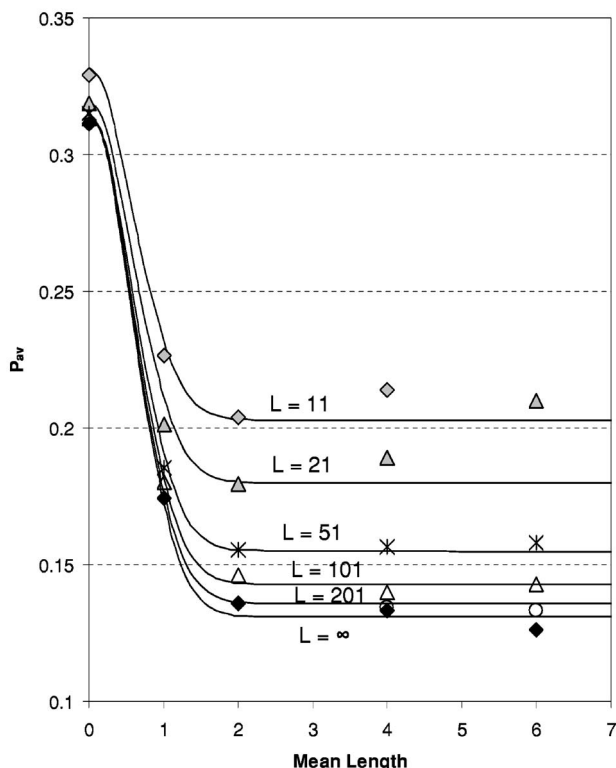


FIG. 1. Average percolation threshold  $p_{av}$  as a function of mean length  $\Lambda_1$  for various lattice sizes  $L$  (symbols). Lines represented fitted functions from Eq. (17).

functions, respectively, using the fixed- $\nu$  method with relatively small  $L=16, 32$ , and  $64$ , and based on only ten realizations.

#### Finite-sized average percolation thresholds $p_{av}$

Figure 1 shows estimates of  $p_c$  and  $p_{av}$  as a function of mean length  $\Lambda_1$  at various lattice sizes  $L$ . In all cases, the 95% confidence interval for  $p_{av}$  is less than 0.001 (not shown). Due to the finite-size scaling property [Eq. (14)], smaller lattices yield larger values for  $p_{av}$ . At short mean lengths ( $\Lambda_1 \leq 2$ ) both the derived percolation threshold  $p_c$  for the infinitely sized domain and  $p_{av}$  of the finite-sized domains decrease rapidly with increasing  $\Lambda_1$ . The range of  $\Lambda_1$  over which the initial decrease of  $p_{av}(\Lambda_1)$  occurs is limited to the interval  $0 \leq \Lambda_1 \leq 4$  and is largely independent of the lattice size. This can be confirmed by fitting a modified Gaussian function to the measured data in Fig. 1 (modified from Mendelson [16]):

$$p_{av}(L, \Lambda_1) = p_{av}(L, \Lambda_1 = \Lambda_{1,min}) + [p_{av}(L, 0) - p_{av}(L, \Lambda_1 = \Lambda_{1,min})] \exp\{-\alpha(L)\Lambda_1^2\} \quad (18)$$

where  $\Lambda_{1,min}$  is the mean length at which the lowest value of  $p_{av}$  is observed, and  $\alpha(L)$  is the slope parameter of  $p_{av}(L, \Lambda_1)$ . Originally suggested to vary with  $L$ , I find that  $\alpha=1.5$  is a reasonably close estimate for any  $L$ , indicating that the rate of initial decrease of  $p_{av}$  is strongly controlled by the lattice correlation, not by the lattice size. The ob-

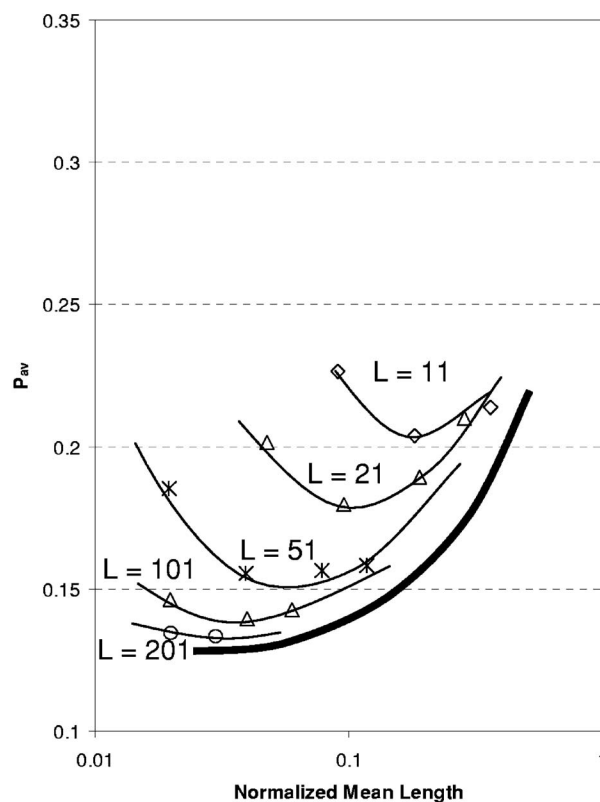


FIG. 2. Average percolation threshold  $p_{av}$  as a function of the logarithm of normalized mean length  $\Lambda_1/L$  for various lattice sizes. Lines are graphically fitted. The thick line represents an approximate lower boundary of  $p_{av}$  for large lattices.

served slope  $\alpha$  is slightly higher than that estimated by Mendelson [16] for a Crossley-Schwartz-Banavar random field [26] or that obtained after fitting Eq. (18) to the three-dimensional (3D) results reported by Renault [15] for spectral random fields with exponential covariances.

The above equation is valid only at small  $\Lambda_1$ . At larger  $\Lambda_1$ , the percolation threshold function  $p_{av}(\Lambda_1)$  of finite lattices does not asymptotically reach a minimum value but increases again after reaching a local minimum near  $\Lambda_{1,min}=2$  or  $\Lambda_{1,min}=4$  (Fig. 1). Similar increases in  $p_{av}(\Lambda_1)$  at larger  $\Lambda_1$  can be observed in the 3D finite-scale simulation results of Renault [15] ( $L=50$ ) and Mendelson [16] ( $L \in \{16, 32, 64\}$ ). This previously unnoticed behavior is a result of the decrease in the relative finite lattice size  $L/\Lambda_1$  as  $\Lambda_1 \rightarrow L$ . In correlated lattices, the finite-size effects are therefore a function of both  $L$  and  $\Lambda_1$  (or, equivalently,  $L$  and  $\lambda$ ). When plotted against the relative mean length  $\Lambda_1/L$ , the apparent location of  $\Lambda_{1,min}/L$  varies for different  $L$  (Fig. 2). The average percolation threshold is affected at levels of  $\Lambda_1/L$  as low as 0.05, even in very large but finite lattices (thick line in Fig. 2).

#### Second moment of $\Pi$

Any measure  $\Delta$  of the spread of the distribution function  $\Pi(p_1)$  is known to scale with  $L^{-1/\nu}$ . For correlated lattices, it is thought that the value of  $\nu$ , and hence the change of

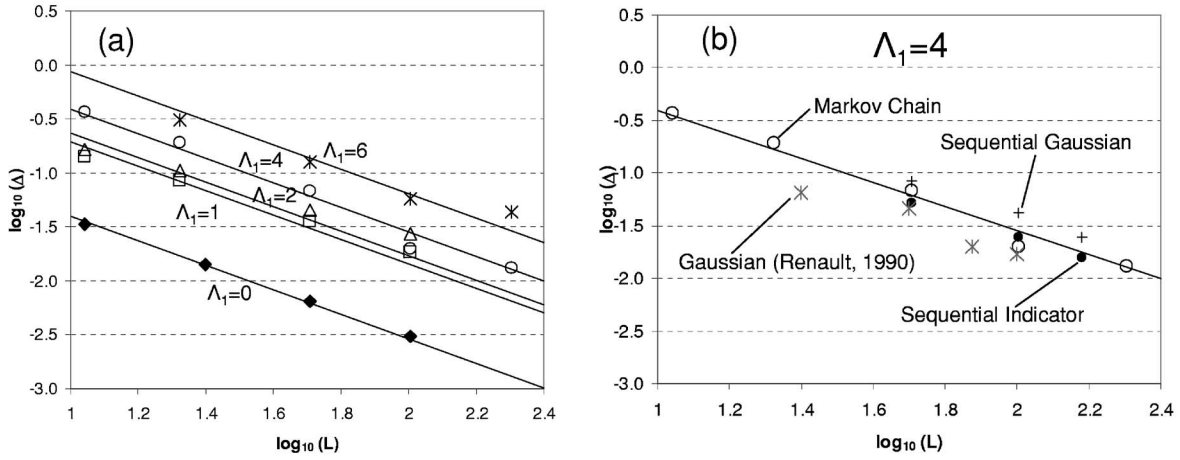


FIG. 3. Finite-size scaling of  $\Delta$  for various mean length  $\Lambda_1$  using the TPMC random field generator (a) and with various random field generators at  $\Lambda_1=4$  (b). Symbols represent empirical results, lines represent best fit to Eq. (13) with  $\nu=0.88$ .

$\log_{10}(\Delta)$  with  $\log_{10}(L)$ , is independent of the correlation or mean length [1,2]. Exact estimates of  $\nu$  by fitting Eq. (14) to measurements of  $\Delta$  are difficult to obtain via Monte Carlo simulation without a very large number of realizations. While I generated on the order of  $10^4$  realizations for smaller lattice sizes, the number of realizations for  $L=101, 201$  was limited to a few hundred to a few thousand. Given the limited accuracy, the results for all  $\Lambda_1$  seem to reasonably fit the scaling value  $\nu=0.88$  [Fig. 3(a)]. Fits are less accurate for  $\Lambda_1=1, 2$ . This may be a limitation of the specific Markov-chain random field generator with the simulated quenching algorithm indicating that it does not perform as accurately at  $\Lambda_1 < 4$  as other binary random field generators.

While  $\nu$  does not significantly change with  $\Lambda_1$ , the magnitude of  $\Delta$  at a given lattice size significantly increases with  $\Lambda_1$  (Table II). In other words, the spread of  $\Pi$  increases with the mean length of the lattice correlation. The observed increase of  $\Delta$  with  $\Lambda_1$ , relative to uncorrelated lattices, is shown to be of similar magnitude for TPMC random fields, sequential indicator random fields, sequential Gaussian random fields, and spectral (turning bands) random fields [15], the latter two of which were converted to indicator random fields prior to the percolation analysis by applying  $p_1$  as a cutoff [Fig. 3(b)].

#### Backbone, cluster size, and connectivity

The scaling behavior of the backbone fraction  $S_\infty$  in correlated TPMC fields, computed at  $p_{av}(\Lambda_1)$ , is consistent with

TABLE II. Prefactors for the scaling relationships (14)–(17) of  $\Delta$ ,  $S_\infty$ ,  $\langle S \rangle$ , and  $\xi^2$  at  $p_{av}$  (Fig. 6) as a function of the scaled mean length  $\Lambda_1$ . Prefactors  $a$  apply to the  $\log_{10}$ -transformed scaling equation  $\log_{10}(Y)=a+(b/\nu)\log_{10}(L)$ , of Eqs. (14)–(17).

$\Lambda_1$	$\log_{10}\Delta$	$\log_{10}\langle S_{inf} \rangle$	$\log_{10}\langle S_{avg} \rangle$	$\log_{10}\langle \xi^2 \rangle$	$\log_{10}\langle \xi_{max}^2 \rangle$
0	-0.265	-0.02	-0.9	-2	-1.15
1	0.43	0.19	-0.6	-2	-1.15
2	0.51	0.38	-0.35	-2	-1.15
4	0.73	0.55	-0.02	-2	-1.15
6	1.08	0.63	0.15	-2	-1.15

that in uncorrelated random fields, for which  $\beta$  was found to be 0.41 [Fig. 4(a)]. Like the spread of  $\Pi$ , the backbone fraction  $S_\infty$  increases with mean length of the lattice correlations. The increase of the backbone fraction decelerates with increase in  $\Lambda_1$  [Fig. 4(a)]. For  $\Lambda_1=4$  and 6, backbone fractions at  $L=11$  and 21, respectively, are significantly lower than expected by the scaling law indicating that the TPMC algorithm is not sufficiently accurate when simulating a lattice that is small relative to the mean length of the lattice correlations.

Mean cluster size  $\langle S \rangle$  and measures of  $\langle \xi \rangle$  for nonspanning clusters also fit known finite-size scaling relations [Eqs. (15) and (16)]. Like  $p_{av}$ ,  $\Delta$ , and  $S_\infty$ , the mean cluster size of nonspanning clusters depends on  $\Lambda_1$ : longer spatial correlations increase the mean cluster size [Fig. 4(b)].

In contrast, the squared radius of gyration of nonspanning clusters does not depend on mean lengths (Fig. 5). The squared radii of gyration of nonpercolating clusters at given lattice size are nearly identical for all  $\Lambda_1 \in \{1, 2, 4, 6\}$ . For the average squared radius of gyration of the largest 30 nonspanning clusters I obtain the following scaling relationship, regardless of mean length or correlation scale of the random field:

$$\log_{10}\langle \xi^2 \rangle = -2.0 + (\gamma/\nu)\log_{10}(L). \quad (19)$$

For the largest nonspanning cluster, the radius of gyration is always

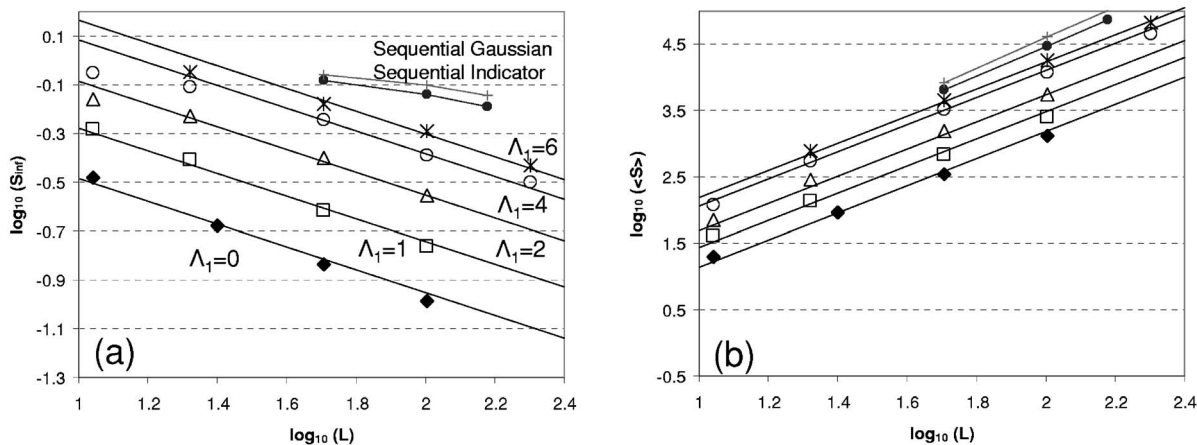


FIG. 4. Finite-size scaling of the infinite cluster (a) and of the average nonpercolating cluster size (b) at various mean length  $\Lambda_1$ . Symbols represent empirical results, lines represent best fit to Eq. (14) (a) and Eq. (15) (b) with  $\nu=0.88$ ,  $\beta=0.41$ , and  $\gamma=1.8$ .

$$\log_{10}\langle \xi_{max}^2 \rangle = -1.15 + (\gamma/\nu)\log_{10}(L), \quad (20)$$

where  $\gamma=1.8, \nu=0.88$ . Moreover, these radii very closely matched those obtained from sequential indicator and Gaussian-derived indicator random fields (Fig. 5). Note that the sample moments for  $\xi^2$  and  $\xi_{max}^2$  were computed regard-

less of the existence of a spanning cluster in a given realization. At  $p_{av}$ , where half the simulations have spanning clusters, the mean squared radius of gyration of the largest nonspanning clusters in nonpercolating realizations is found to be always  $10^{0.3}$  times larger than that in realizations with a spanning cluster:

$$\log_{10}\langle \xi_{max}^2 \rangle = -1.0 + (\gamma/\nu)\log_{10}(L) \quad \text{if no spanning cluster exists,} \quad (21)$$

$$\log_{10}\langle \xi_{max}^2 \rangle = -1.3 + (\gamma/\nu)\log_{10}(L) \quad \text{if a spanning cluster exists.} \quad (22)$$

Equivalently, the mean radius of gyration of the largest nonspanning clusters is found to be

$$\log_{10}\langle \xi_{max} \rangle = -0.54 + 1.05 \log_{10}(L) \quad \text{if no spanning cluster exists,} \quad (23)$$

$$\log_{10}\langle \xi_{max} \rangle = -0.74 + 1.05 \log_{10}(L) \quad \text{if a spanning cluster exists.} \quad (24)$$

For the mean radius, the slope is slightly larger than the theoretically expected unit slope [ $\nu/\nu$ , Eq. (17)]. Similar differences between percolating vs nonpercolating realizations are observed for  $\langle S \rangle$ .

Prefactors of the scaling functions (Table II) increase with  $\Lambda_1$ , i.e., with the relative discretization of the correlated structures in a heterogeneous medium. It appears that the prefactors of the scaling functions for  $S_\infty$  and  $\langle S \rangle$  reach an asymptotic value at some  $\Lambda_1 > 6$  (Fig. 6).

### DISCUSSION AND CONCLUSION

Our results provide closure to and expand upon the observations by Silliman *et al.* [14], Renault [15], and Mendelson [16], the first two of which were inspired by the common application of numerical methods to the study of (three-dimensional) physical phenomena in correlated random media, specifically the simulation of flow and transport pro-

cesses in permeable geologic media. In the stochastic analysis of effective properties of such media, much attention has been given to the role of statistical properties of random media, particularly spatial two-point statistics or geostatistics, to the simulation of such random media given specific low-order statistical properties [22], and to the effective flow and transport properties of such media [12,27]. While it is well known that such effective, large-scale properties are highly dependent on the percolation properties of random media, comparatively little research has been directed toward quantifying such finite-size percolation effects in three-dimensional systems.

The results presented here illustrate the importance of properly discretizing observed heterogeneity with short-range correlations in numerical modeling of percolation-dependent processes in heterogeneous media: if the grid discretization is too coarse ( $\Lambda_1 < 4$ ), the simulated percolation threshold is higher than that of the actual heterogeneous me-

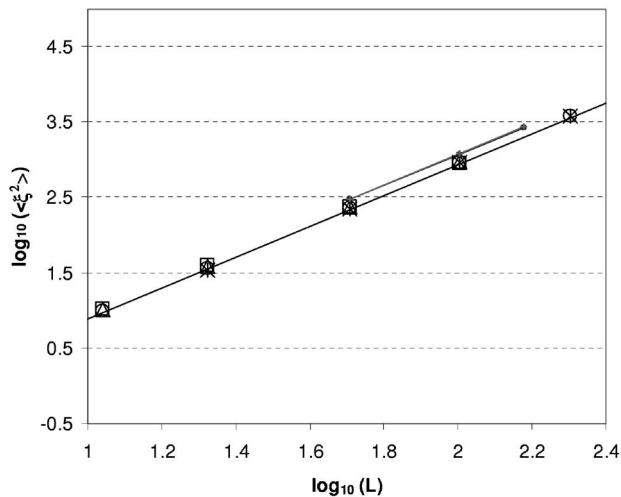


FIG. 5. Finite-size scaling of the mean squared radius of gyration as a function of mean length  $\Lambda_1$  and random field generator (same symbols as in Fig. 4). Lines represent the scaling relationship (19).

dia. Similarly, if the simulated domain is too small relative to the mean length or correlation length ( $\Lambda_1/L > 0.05$ ), the simulated percolation threshold may also be higher than in the actual finite-sized medium (if the simulated domain represents only a subdomain of the actual finite-sized medium).

Numerical studies of disordered media processes (e.g., by the finite difference method [12]) are typically based on lattices with  $10^4$ – $10^6$  nodes if implemented in three dimensions, yielding typical lattice lengths  $L$  on the order of  $10^{1.33}$  to  $10^2$ . With minimum discretization requirements being such that  $\Lambda_1 = 4$  [13,27], the relative lattice size  $L/\Lambda_1$  or  $L/\lambda$  of the simulated domain is typically limited to 10–30. For numerical studies of disordered media processes, it is therefore critical to take into account finite-size effects on percolation and on the associated phase connectivity properties of lattices. Note that if relative domain size or relative discretization is chosen differently for different directions in a multidimensional simulation domain, the results may show an apparent anisotropy due to the different magnitude of finite-size and discretization effects on percolation in different directions. To avoid such effects, both relative discretization

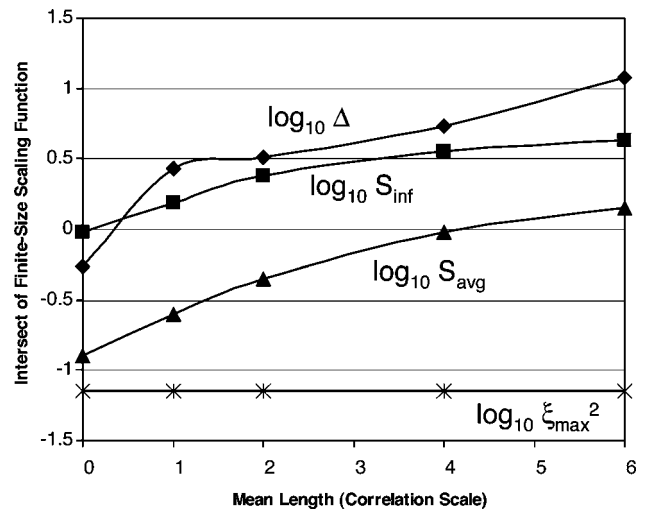


FIG. 6. Prefactors (zero intersects) obtained from the fits to the finite-size scaling relationships shown in Figs. 3–5.

and relative domain size should be identical in all directions or large enough to avoid discretization and size effects.

Like other random fields with short-range correlations, the results confirm that Markov-chain random fields belong in the same universality class as uncorrelated random fields. At 12.6%, the theoretical percolation threshold  $p_c$  for an infinite lattice is similarly low as that found for other random fields with short-range correlations. In heterogeneous media with relative finite system lengths  $L/\Lambda_1$  of less than 20, the average percolation threshold  $p_{av}$  is higher and increases with decreasing heterogeneous media dimension  $L/\Lambda_1$ . For specific numerical applications on finite-sized, correlated grids representing cubic lattices, Table II in conjunction with Eq. (12) and the scaling functions (13)–(17), (19), and (20) yield reasonable estimates of  $\Pi$  at any  $p_1$  and of  $S_\infty$ ,  $\langle S \rangle$ , and  $\xi^2$  at  $p_{av}$ .

#### ACKNOWLEDGMENTS

Funding for this work was provided by the Collaborative UC/Los Alamos Research program (University of California Directed Research Development). The author would like to thank Nazrul Islam and Ayman Ahmed at the University of California, Davis, for their programming support.

- [1] Muhammad Sahimi, *Applications of Percolation Theory* (Taylor and Francis, Bristol, PA, 1994).
- [2] Dietrich Stauffer and Amnon Aharony, *Introduction to Percolation Theory*, 2nd ed. (Taylor and Francis, Philadelphia, PA, 1994).
- [3] A. Weinrib, *Phys. Rev. B* **29**, 387 (1984).
- [4] Muhammad Sahimi and Sumit Mukhopadhyay, *Phys. Rev. E* **54**, 3870 (1996).
- [5] Sona Prakash, Shlomo Havlin, Moshe Schwartz, and H. Eugene Stanley, *Phys. Rev. A* **46**, R1724 (1992).
- [6] H. Mueller-Krumbhaar, *Phys. Lett.* **50A**, 27 (1974).

- [7] A. Coniglio, C. R. Nappi, F. Peruggi, and L. Russo, *J. Phys. A* **10**, 205 (1977).
- [8] L. M. de Moura and Raimundo R. dos Santos, *Phys. Rev. B* **45**, 1023 (1992).
- [9] C. M. Chaves and Belita Koiller, *Physica A* **218**, 271 (1995).
- [10] A. M. Vidales, R. J. Faccio, J. Riccardo, E. N. Miranda, and G. Zgrablich, *Physica A* **218**, 19 (1995).
- [11] A. J. Ramirez-Cuesta, R. J. Faccio, and J. L. Riccardo, *Phys. Rev. E* **57**, 735 (1998).
- [12] D. Zhang, *Stochastic Methods for Flow in Porous Media* (Academic Press, San Diego, 2002).

- [13] Graeme W. Milton, *The Theory of Composites* (Cambridge University Press, Cambridge, U.K., 2002).
- [14] S. E. Silliman, *J. Hydrol.* **113**, 177 (1990).
- [15] Pierre Renault, *Transp. Porous Media* **6**, 451 (1991).
- [16] Kenneth S. Mendelson, *Phys. Rev. E* **56**, 6586 (1997).
- [17] A. Elfeki and M. Dekking, *Math. Geol.* **33**, 569 (2001).
- [18] G. S. Weissmann, S. F. Carle, and G. E. Fogg, *Water Resour. Res.* **35**, 1761 (1999).
- [19] Steven F. Carle and Graham E. Fogg, *Math. Geol.* **28**, 453 (1996).
- [20] Steven F. Carle, computer code T-PROGRS: Transition Probability Geostatistical Software Version 2.1, available from the author at carle1@llnl.gov
- [21] Steven F. Carle and Graham E. Fogg, *Math. Geol.* **29**, 891 (1997).
- [22] C. V. Deutsch and A. G. Journel, *GSLIB: Geostatistical Software Library and User's Guide* (Oxford University Press, New York, 1992).
- [23] Harvey Gould and Jan Tobochnik, *An Introduction to Computer Simulation Methods*, Part 2 (Addison-Wesley, Reading, MA, 1988).
- [24] D. A. Wollman, M. A. Dubson, and Qifu Zhu, *Phys. Rev. B* **48**, 3713 (1993).
- [25] P. R. A. Campos, L. F. C. Pessoa, and F. G. Brady Moreira, *Phys. Rev. B* **56**, 40 (1997).
- [26] P. A. Crossley, L. M. Schwartz, and J. R. Banavar, *Appl. Phys. Lett.* **59**, 3553 (1991).
- [27] Yoram Rubin, *Applied Stochastic Hydrogeology* (Oxford University Press, Oxford, U.K., 2003).